

# Environmental Science Nano

Accepted Manuscript



This is an *Accepted Manuscript*, which has been through the Royal Society of Chemistry peer review process and has been accepted for publication.

*Accepted Manuscripts* are published online shortly after acceptance, before technical editing, formatting and proof reading. Using this free service, authors can make their results available to the community, in citable form, before we publish the edited article. We will replace this *Accepted Manuscript* with the edited and formatted *Advance Article* as soon as it is available.

You can find more information about *Accepted Manuscripts* in the [Information for Authors](#).

Please note that technical editing may introduce minor changes to the text and/or graphics, which may alter content. The journal's standard [Terms & Conditions](#) and the [Ethical guidelines](#) still apply. In no event shall the Royal Society of Chemistry be held responsible for any errors or omissions in this *Accepted Manuscript* or any consequences arising from the use of any information it contains.

## Transformations of Oxidized Multiwalled Carbon Nanotubes Exposed to UVC (254nm) Irradiation

Julie L. Bitter,<sup>a</sup> Jin Yang,<sup>b</sup> Somayeh Beigzadehmilani,<sup>c</sup> Chad Jafvert,<sup>c</sup> and  
D. Howard Fairbrother,<sup>a1</sup>

<sup>a</sup> Department of Chemistry, Johns Hopkins University, Baltimore, MD 21218

<sup>b</sup> Department of Geography & Environmental Engineering, Johns Hopkins University,  
Baltimore, MD 21218

<sup>c</sup> School of Civil Engineering, Purdue University, West Lafayette, IN 47907

*Revision date: May 30, 2014; prepared for publication as an Article in  
*Environmental Science: Nano**

### Abstract

Motivated by the ability of UVC radiation to destroy harmful pathogens in drinking and waste water treatment plants, we have investigated the effect of 254nm (UVC) radiation on the physical and chemical properties of oxidized multiwalled carbon nanotube (O-MWCNT) suspensions. Absorbance and particle size measurements were employed to monitor suspension stability, while X-ray photoelectron spectroscopy (XPS), transmission electron microscopy (TEM), and Raman spectroscopy were used to characterize chemical and structural transformations. Experimental results indicate that after an initial period of irradiation where suspensions remained stable, exposure to 254nm light caused O-MWCNT particles to aggregate. The duration of this initial period of particle stability increased at higher pH and lower ionic strength. This photo-induced aggregation was found to be the result of a loss of negatively charged carboxylic acid functional groups. Experiments performed in solutions containing different levels of dissolved oxygen, used to alter the concentration of reactive oxygen species (ROS) present during irradiation, indicate that ROS are not directly involved in the photodecarboxylation process. However, our results are consistent with a direct single photon decarboxylation process, previously identified in the organic photochemistry literature as the mechanism for CO<sub>2</sub> removal from small organics molecules. Photodecarboxylation proceeded in the absence of any significant mass loss or changes in the O-MWCNT structure. Thus, UVC irradiation was unable to mineralize carbon atoms in the core of the O-MWCNTs, although it transformed the physical state of O-MWCNTs by changing the surface chemistry.

---

<sup>1</sup> To whom correspondence should be addressed. email: howardf@jhu.edu

## Introduction

The rapidly expanding use of nanoparticles (NPs), such as carbon nanotubes (CNTs), nano-silver, and nano-scale metal oxides in consumer products has prompted research into the potential health and safety effects of these NPs when they are released into the environment.<sup>1-9</sup> NPs could enter the environment from various point sources during industrial manufacturing as a result of spills that occur during transport, or from the degradation of NP-containing products (e.g. polymer nanocomposites) at various stages of their life cycle.<sup>2</sup> Once NPs enter the environment they can undergo physical and/or chemical transformations. Possible chemical transformations include degradation of surface coatings, oxidation/reduction as a result of exposure to concomitant chemicals such as hydroxyl radicals, ozone, or sulfides, or biotransformations when NPs are exposed to cellular enzymes and proteins. All of these transformation processes could modify a NP's environmental behavior (e.g. transport, aggregation state, toxicity) with a direct impact on their environmental health and safety effects.<sup>10</sup> Consequently, it is important to understand the nature and kinetics of transformations that occur to NPs.

Photolysis of carbon based nanomaterials, such as fullerenes, graphene oxide nanosheets, and carbon nanotubes, is one of the most important and widely studied transformation processes.<sup>11-26</sup> Depending on the original state of the carbon surface, the overall effect of photolysis appears to fall into one of two categories, oxidation or reduction. When the carbon surface is pristine or unfunctionalized, previous studies have shown that photolysis often results in the introduction of oxygen containing functional groups. For example, in the case of fullerene clusters ( $nC_{60}$ ) exposed to UV light in water, oxidation of the surface under either anoxic<sup>11</sup> and oxic<sup>12</sup> conditions reduces aggregate size. This effect is postulated to be a result of the fullerenes becoming more hydrophilic as a result of surface oxidation.<sup>11, 13</sup> Similarly, when unfunctionalized (pristine) CNTs are irradiated with UV light, photo-induced oxidation has been observed. For example, Savage *et al.* studied the adsorption of oxygen to pristine MWCNT films in air exposed to both ambient light and 240nm UV irradiation.<sup>14</sup> They used thermoelectric power (TEP) as their gauge, where TEP values are negative for n-type conductors and positive for p-type conductors. Measured TEP values from the MWCNT films became more positive the longer the films were photolyzed in an oxygen-containing environment. The authors argued that MWCNTs were being oxidized under these conditions, and that oxygen was adsorbing preferentially at defects in the CNT sidewalls. Similar results were obtained by Alvarez *et al.*<sup>15</sup> and Lee *et al.*<sup>16</sup> when they exposed pristine single walled CNTs (SWCNTs) to UV irradiation, and showed with X-ray photoelectron spectroscopy (XPS) that an increase in the surface oxygen content after UV exposure. These findings were supported with attenuated total reflection-Fourier transform infrared spectroscopy (ATR-FTIR) data which suggested that the oxygen introduced was predominantly in the form of hydroxyl groups.

In contrast, photoreduction appears to be the dominant transformation when the carbon surface is oxidized prior to photolysis. For example, suspensions of graphene oxide (GO) nanosheets exposed to UVA-visible irradiation (310 – 450nm)<sup>17-22</sup> have shown a decrease in epoxide and hydroxyl groups, as measured by XPS and IR. These chemical transformations are also cited to be responsible for the obvious differences in the physical structure of irradiated and unexposed GO nanosheets observed by AFM and TEM, with large defect areas present after irradiation. This effect has been attributed to the photo-induced removal of peripheral carbonyl

and hydroxyl groups upon UVA irradiation ( $\lambda = 350\text{nm}$ ).<sup>22</sup> The results are consistent with data from Smirnov *et. al.*, who used mass spectrometry to detect the evolution of H<sub>2</sub>O, CO, O<sub>2</sub>, and CO<sub>2</sub> from the surface of GO films.<sup>18</sup> Matsumoto *et. al.* proposed mechanisms for the evolution of these gases involving the excitation of the  $\pi$ - $\pi^*$  band to produce holes and electrons that would facilitate the removal of CO<sub>2</sub> and H<sub>2</sub>O from the GO nanosheets.<sup>17</sup>

Photochemical transformations have also been observed when oxidized CNTs are photolyzed. For example, Chen and Jafvert examined carboxylated SWCNTs in water exposed to sunlight irradiation and 350nm lamp light.<sup>23, 24</sup> The oxidized SWCNTs (O-SWCNTs) aggregated after irradiation under conditions where O-SWCNTs are normally stable. They also observed production of ROS in the form of singlet oxygen, superoxide radicals, and hydroxyl radicals from as-received and acid-washed carboxylated SWCNTs. In a related study, Hwang *et. al.* used 300-400nm (UVA) irradiation to study carboxylated MWCNT suspensions in water with mono and divalent salts.<sup>25</sup> A loss of surface oxygen content was observed by XPS when oxidized MWCNTs were irradiated with UVA light. This loss in oxygen resulted in aggregation and deposition of MWCNTs as measured by time resolved dynamic light scattering (TR-DLS) and quartz crystal microbalance (QCM-D), respectively. A related study by the same researchers, also conducted with UVA light saw a loss of oxygen in the form of carboxylic acid functional groups and an increase in the structural disorder, monitored by XPS and Raman, respectively. The addition of hydrogen peroxide was observed to enhance the rate of CNT aggregation, an effect that was attributed to reactions of reactive oxygen species (ROS) with carboxylic acid groups on the CNT surfaces.<sup>26</sup>

To date, studies on the photolysis of CNTs have focused on the effect of visible light and lower energy UVA light. In contrast, comparatively little is known about the effects of more energetic UVC irradiation used in drinking and waste water treatment plants. UVC light has the potential to directly excite electronic transitions (e.g.  $\pi$ - $\pi^*$  transitions) and open up new transformation pathways, including complete NP mineralization. This has motivated us to study the effects of UVC light on oxidized multi-walled carbon nanotubes (O-MWCNTs) under various solution conditions (e.g. pH, ionic strength, dissolved oxygen) as a function of irradiation time and light intensity. The concentration and size of suspended particles were measured with UV-Vis and DLS respectively as a function of irradiation time, while chemical and physical transformations were evaluated using complementary analytical techniques including mass loss, TEM, Raman, and XPS with chemical derivatization. Questions we sought to address included, (1) what are the fundamental physical and chemical transformations of oxidized MWCNTs that occur when they are exposed to UVC irradiation? (2) how do water quality parameters affect the rate of transformation? (3) can UVC mineralize oxidized MWCNTs? and (4) can we provide insights into the mechanism of the transformation processes?

## Experimental

### *O-MWCNTs*

Two types of commercially available O-MWCNTs were used for this study. The majority of the studies were performed with O-MWCNTs purchased from NanoLab, Inc. (Newton, MA) that had been oxidized by the manufacturer using a 3:1 sulfuric:nitric mixture (PD15L5-20-COOH, outer diameter: 15+/-5nm, Length: 5-20 $\mu$ m, Purity: >95%). These O-MWCNTs were subject to a rigorous cleaning procedure outlined in Smith et. al.<sup>27-29</sup> In brief, the O-MWCNTs first underwent repeated rinsing/centrifugation cycles with deionized water. Then 4M NaOH was used to remove amorphous carbon. 4M HCl was added next to neutralize the solution, and finally repeated rinses with DI water were performed to remove the electrolytes from the supernatant. The sample was judged free of electrolyte when the resistivity of the supernatant reached >0.5M $\Omega$ . Post cleaning, the CNTs were dried on a microscope slide, scraped off, and ball-milled for homogeneity. Cleaned and dried CNTs were stored in small clean screw cap vials prior to preparing colloidal suspensions and subsequent photolysis experiments. Principally as a point of comparison and to explore the generality of our results, we also used oxidized MWCNTs (MWCNT-OH, outer diameter: 10-20nm, Length: 10-30 $\mu$ m, Ash: <1.5%, Purity: >95%) purchased from Cheaptubes (Brattleboro, VT).

### *Chemicals*

Sodium chloride, sodium hydroxide, sodium dihydrogen phosphate, and sodium hydrogen phosphate were purchased from Fisher Scientific and used without purification. Nitric acid, hydrochloric acid, and the derivatizing agents 2,2,2-trifluoroacetic anhydride (TFAA), 2,2,2-trifluoroethanol (TFE), N,N'-di-tert-butyl-carbodiimide (DTBC), and 2,2,2-trifluoroethylhydrazine (TFH) were all purchased from Sigma-Aldrich and used without further purification. HPLC-grade ultrapure water was purchased from VWR International and used as received. Ultra-high purity oxygen and nitrogen were purchased from Air Gas (Malvern, PA).

### *Preparation of O-MWCNTs Suspensions*

Stock suspensions of O-MWCNTs were prepared by adding a known mass (4 – 6mg) of the desired O-MWCNTs to 200mL of HPLC-grade ultrapure water. Samples were then sonicated for 20hrs (Branson 1510, 70W). After sonication, suspensions were centrifuged at 1000rpms for 5min to remove any glass etched from the walls of the flask, and any O-MWCNTs that were not taken up into suspension (i.e., MWCNT bundles, amorphous carbon, very lowly oxidized MWCNTs). This stock suspension was then transferred to clean 200mL Pyrex containers for storage. Previous studies have shown that this procedure yields a large concentration of individual O-MWCNTs in suspension.<sup>30</sup>

A Varian Cary 50 UV-Vis was used to determine the absorbance of stock O-MWCNT suspensions. Prior to photolysis, a known aliquot of the stock was diluted to 1.25mg C/L. UV-Vis was used to ensure that the absorbance of the suspension was constant across different experiments. The absorbance of the suspensions used for irradiation experiments was set to 0.34 at 350nm (this corresponds to approximately 5mg C/L for oxidized NanoLab MWCNTs). A typical UV-Vis of a Nanolabs O-MWCNT suspension is shown in Figure S1. Similar UV-Vis

spectra were obtained for the Nanolabs and Cheap Tubes O-MWCNTs.

The ionic strength was controlled by adding appropriate volumes of a 4M NaCl stock solution while the pH ( $\pm 0.1$ ) was set using phosphate buffer (3mM final concentration) and small quantities (in increments of 10 – 20 $\mu$ L) HCl or NaOH as needed. Preliminary experiments revealed that in the absence of a buffer, the pH of the suspension decreased during irradiation, destabilizing the O-MWCNTs particles and obscuring the effect of UVC radiation. The use of a buffer was therefore necessary to stabilize the pH throughout an experiment, enabling us to isolate the effect of different variables (pH, ionic strength, light intensity) on particle stability. A triprotic phosphate buffer was chosen because it did not absorb in the region of interest (between 250 – 350nm), could be used over the range of pH values studied (4 – 10), and would not be affected by the presence of CO<sub>2</sub>, unlike carbonate buffers. Control studies conducted with phosphate and acetate buffers were used to verify that the phosphate buffer did not change the effect or kinetics of UVC exposure (Figure S2).

Prior to UVC photolysis, initial particle size measurements were performed by removing a 0.5mL aliquot from the suspension, before being diluted to 1.25mg C/L with buffered and pH balanced ultrapure water. Particle size measurements were carried out in disposable plastic cuvettes at 24°C with a Malvern ZetaSizer Nano-ZS using a 5mW He-Ne laser (633nm). A non-invasive backscattering configuration (detection angle 173° with respect to the incident laser light) was used to collect measurements. Effective hydrodynamic diameters were modeled by the Stokes-Einstein relationship developed for spherical particles and represent the average of five separate measurements, each consisting of 10-15 scans.

Once absorbance and particle size measurements confirmed that a stable and appropriately concentrated O-MWCNT suspension had been prepared, samples were transferred to a large quartz vessel or a quartz test tube (see below for details). These vessels were then purged with ultra-high purity oxygen or nitrogen before being sealed first with Parafilm and then with aluminum foil. Before being exposed to UVC irradiation, the outside surface of the quartz glassware was wiped clean with acetone to remove any dust and oils that may interfere with the way the light passes through the glassware.

#### *UVC Irradiation*

Colloidal suspensions of O-MWCNTs were irradiated in an RPR-100 Rayonet UV photochemical reaction chamber equipped with sixteen, 35W low pressure mercury lamps (>90% 254nm emission, irradiance with all 16 lamps = 15.4 – 16.0 mW/cm<sup>2</sup>), purchased from Southern New England Ultraviolet (Branford, CT). Most experiments were performed with 16 lamps (photon flux  $\sim 1.32 \times 10^{17}$  quanta/sec as measured by actinometry). For experiments performed with less than 16 lamps, some lamps were wrapped with aluminum foil. A symmetric pattern of wrapping was adopted to ensure uniform light distribution around the entire chamber. Photon flux measurements obtained for different numbers of exposed (unwrapped) lamps can be found in Figure S3 and Table S1.

UVC irradiation experiments were performed in one of two configurations:

(i) Large Batch Volumes: A 600mL or 1000mL quartz beaker was used to ensure that

enough O-MWCNTs were present for surface characterization and mass loss measurements following UVC irradiation. In these experiments a beaker was set on a stand inside the chamber so that the sides of the glassware sat at a height equal to the midpoint of the lamps for maximum exposure. O-MWCNT suspensions were irradiated in this static configuration until UVC-induced aggregation and settling had occurred. At this point a small amount of concentrated HCl was added to the beaker to aid in the removal of any remaining suspended CNTs. The contents of the beaker were then centrifuged (4000rpms for 10min), and the supernatant was decanted and collected in a clean 1L Pyrex bottle. The O-MWCNTs collected in the test tubes were then rinsed thoroughly with DI water until the resistivity of the supernatant was  $>0.5\text{M}\Omega$  and dried on a cleaned glass microscope slide overnight at  $70^\circ\text{C}$ . The mass of O-MWCNTs remaining after irradiation was determined by scraping the dried O-MWCNTs off the glass and weighing them on aluminum foil that had been deionized to remove static charge. Mass loss was determined by comparing the values obtained from UVC irradiated O-MWCNT samples to control studies, where suspensions of O-MWCNTs had been prepared and then removed from solution by adding sufficient acid to destabilize particles without any UVC exposure. O-MWCNTs generated from control and irradiation studies were also used for surface characterization.

(ii) Small Sample Volumes: These experiments were used to measure changes in particle concentration (absorbance) and size as a function of irradiation time. A dozen 15mL quartz test tubes were placed in a rotating carousel within the Rayonet and exposed to UVC irradiation. The test tubes were placed into a rotating 12-slot carousel set to a height at the midpoint of the UVC lamps to ensure that each test tube received uniform exposure. Quartz test tubes were removed after discrete exposure times and analyzed for changes in particle size and concentration. Each time a test tube was removed we checked that the pH and conductivity remained unchanged from the initial time point. A replacement (containing an already sampled suspension of O-MWCNTs) was inserted into the place vacated to maintain uniform light intensity within the carousel. Because the effects of light intensity were studied with this set-up the absolute light intensity experienced by the O-MWCNTs was also calibrated for these experiments (see below).

For each O-MWCNT suspension removed from the carousel, a 0.5mL aliquot was extracted from the top of the test tube (taking care not to shake or disturb the contents) and placed into a clean 5mL screw cap vial. For particle size measurements, the 0.5mL aliquot was diluted to 1.25mg C/L with ultrapure buffered water and analyzed using a Malvern ZetaSizer Nano-ZS. To complement particle size measurements UV-Vis was used to determine the concentration of O-MWCNTs remaining in suspension. In this analysis the O-MWCNT suspension was gently centrifuged (1000rpms) for 3 minutes to remove any large aggregates that would otherwise compromise absorbance measurements by excessive scattering. An aliquot of the centrifuged O-MWCNT suspension was then pipetted into a quartz cuvette and the UV-Vis spectra measured from 200 – 900nm in a Varian Cary 50 UV-Vis spectrophotometer. Five separate readings were taken and the average absorbance at 350nm used to determine the O-MWCNT particle concentration.

#### *Calibration of UVC Light Intensity*

To determine the UVC light intensity experienced by the O-MWCNTs during irradiation, actinometry was performed using potassium ferrioxalate as a colorimetric indicator. Light causes the decomposition of ferrioxalate, liberating  $\text{Fe}^{2+}$  ions. The addition of o-phenanthroline causes

the  $\text{Fe}^{2+}$  ions to form a red colored complex with an absorption maximum at 510nm. By measuring the absorbance of this complex it is possible to determine the  $\text{Fe}^{2+}$  concentration. Since the quantum efficiency of the ferrioxalate decomposition at 254nm is well known this information allows us to quantify the UVC light intensity.<sup>31</sup> More comprehensive details regarding the calibration of the photochemical reactor can be found in the Supporting Information.

#### *Characterization of O-MWCNT Powders*

O-MWCNTs were analyzed before and after UVC exposure to determine the effect of irradiation on both the chemical and structural characteristics of the NPs.

**Chemical characterization:** To determine surface composition, a small sample of powdered O-MWCNTs was pressed onto a 1cm x 1cm piece of double sided copper tape that was adhered to an XPS sample stub, ensuring no copper was visible. A PHI 5400 XPS system using Mg  $K\alpha$  x-ray (1253.6eV) irradiation was used to analyze O-MWCNT samples. A high energy electron analyzer operating at a constant pass energy was used to measure the ejected photoelectrons. Elemental quantification was performed using a pass energy of 178.95eV at a scan rate of 0.25eV/step. O-MWCNT samples were analyzed for total oxygen content as well as oxygen functional group distribution using wet chemical derivatization techniques previously used to study CNTs in our lab.<sup>32, 33</sup> In brief this method uses fluorine-containing reagents (2,2,2-trifluoroacetic anhydride (TFAA), 2,2,2-trifluoroethanol (TFE), and 2,2,2-trifluoroethylhydrazine (TFH)) to selectively and quantitatively tag specific functional groups. XPS data was analyzed by commercial software (CasaXPS).

**Structural characterization:**

(i) TEM: O-MWCNTs were prepared for TEM analysis by dipping a holey-carbon TEM grid into O-MWCNT-containing suspensions and allowing them to dry in air. The grids were then imaged using a Philips CM 300 field emission gun TEM operating at 297kV. A CCD camera mounted on a GIF 200 electron energy loss spectrometer was used for image collection.

(ii) Raman: Dried O-MWCNT samples were mounted onto a microscopic slide and analyzed by Raman spectroscopy over 10 second exposure times with 3 spectral averages using an XploRA ONE Raman system from Horiba Scientific (Edison, NJ). A solid state Nd:YAG laser (50mW) emitting an excitation wavelength of 532 nm was used with 100x objective. Samples were scanned over the range of 500 – 3000  $\text{cm}^{-1}$ . Instrument parameters include: slit = 200  $\mu\text{m}$ , hold= 300, grating = 1800, filter = 10%.

## Results and Discussion

### *Visual Effect of UVC Irradiation*

An example of the visual changes that occurred to oxidized multi-walled carbon nanotubes (O-MWCNTs) as a function of UVC irradiation time is shown in Figure 1. For an initial period of irradiation the suspension displays little visible change in color or appearance. However, beyond a certain irradiation time (greater than 16 hours in Figure 1) the O-MWCNTs begin to aggregate, first forming visible particulates and then eventually larger, settleable aggregates, and for sufficiently long irradiation times the supernatant becomes clear to the naked eye. The qualitative effect of UVC irradiation shown in Figure 1 was observed for all of the experiments reported in this study, although the time scale for aggregation to occur depended upon the water quality parameters, characteristics of the O-MWCNTs used, and the light intensity. Separate irradiation studies conducted in the Rayonet on colloidal suspensions in quartz vessels wrapped with aluminum foil (dark controls) showed no change in absorbance or particle size, revealing that the transformations were strictly a result of UVC exposure (see Figure S4). The CNT aggregation and settling observed in this study are qualitatively consistent with previous findings that studied carboxylated single walled<sup>23</sup> and multiwalled CNTs<sup>25</sup> exposed to UVA irradiation.

UVC induced phototransformations were examined more quantitatively by acquiring absorbance and particle size measurements using UV-Vis and DLS, respectively. The UV-Vis absorbance profile for suspensions of O-MWCNTs (Figure S1) are similar to previous studies<sup>25</sup> with a broad peak at  $\lambda = 264\text{nm}$ , corresponding to the  $\pi \rightarrow \pi^*$  transition in the conjugated sidewall ring structure.<sup>34, 35</sup> The sharp increase seen at wavelengths approaching  $\lambda = 200\text{nm}$  is due to the phosphate buffer and NaCl (see Figure S5) although these absorbance features do not overlap with the output of UV light and do not influence the results obtained in the present study.<sup>36</sup> As the UVC irradiation time increases, Figure S1 shows that the intensity of the absorbance profile decreases without any significant changes in shape.

An example of the change in O-MWCNT particle concentration and particle size measured as a function of UVC irradiation time is shown in Figure 2. During the initial stages of irradiation (up to approximately 18 hours in this case) absorbance measurements illustrate that the concentration of O-MWCNTs in suspension remains relatively unchanged, and the average particle size only increases slightly. However, for irradiation times in excess of 24 hours a rapid increase in particle size ( $> 400\text{nm}$ ) is observed and the colloidal O-MWCNT concentration drops sharply. It is during this time (shaded region of Figure 2) that small particulates are observed, and large settleable aggregates begin to form.

### *Effects of Water Quality Parameters*

The effects of water quality were investigated by varying the pH and ionic strength. Figure 3 and Figure S6 illustrate that the resistance of the O-MWCNTs to UVC-induced aggregation increases at lower ionic strength and higher pH values. Thus, for NaCl concentrations of 4 – 5mM, the O-MWCNT absorbance and particle size remains roughly unchanged for irradiation times less than 18hrs. In contrast, for NaCl concentrations of 12mM settleable aggregates are observed after less than 6hrs. In terms of pH effects, at pH 4 (black

triangles) the O-MWCNTs are quickly destabilized by UVC irradiation, with O-MWCNT aggregation being almost complete after less than two hours. In contrast, at pH 10 (green circles) the same particles resisted the effects of UVC-induced aggregation for over 48 hours. These trends in increased resistance to UVC irradiation (low ionic strength, high pH) correspond to the same conditions that increase the stability of negatively charged colloids towards aggregation. It should be noted that O-MWCNT aggregation did not occur over the range of pH and ionic strength values studied in the absence of UVC radiation.

#### *Chemical Transformations to O-MWCNTs caused by UVC Irradiation*

XPS was used to examine chemical changes that occurred to the surface of O-MWCNTs as a result of UVC-induced aggregation. Figures 4A and 4B show a comparison of the C(1s) and O(1s) spectral envelopes obtained from a suspension of O-MWCNTs that were not exposed to UV light (solid red line) and a suspension of the same O-MWCNTs after UVC-induced aggregation (dashed blue line). Although the C(1s) spectral envelope remains virtually unchanged after UVC irradiation, the O(1s) envelope exhibits a noticeable decrease in intensity (from 9%O to 5.9%O). A similar decrease in oxygen was observed for a number of O-MWCNTs under different solution conditions (see Table S2) as a result of UVC-induced aggregation. The decrease in the oxygen signal intensity in the absence of any marked change to the C(1s) profile is a consequence of the fact that all of the oxygen functional groups are located at the surface of the O-MWCNTs, while approximately 68% of the C(1s) signal comes from the carbon core of the O-MWCNTs. This calculation is based on a previous method developed in our group and applied to NanoLabs, Inc. O-MWCNT which has a manufacturer specified average of 10 walls with an interlayer spacing of 0.34nm.<sup>37</sup> Indeed, in previous studies we have shown that even when the concentration of oxygen at the surface of O-MWCNTs more than doubles the C(1s) envelope remains essentially unchanged.<sup>32, 33</sup>

To provide more detailed information on the effect that UVC irradiation has on the surface chemistry of O-MWCNTs we used chemical derivatization to quantify changes in hydroxyl, carboxyl, and carbonyl group densities.<sup>32, 33</sup> Figure 4C shows an example of the results from this analysis. The data reveals that the carboxyl groups, as well as residual (%O<sub>other</sub>) oxygen functionalities such as ethers or esters that could also be present on the O-MWCNT surface but cannot be tagged by chemical derivatization, exhibited a measurable decrease in concentration. The loss of carboxylic acid groups was observed in all of the UVC irradiated O-MWCNTs analyzed by chemical derivatization, indicative of a photodecarboxylation (PDC) process. Although there is some variability in the results obtained on different O-MWCNTs, chemical derivatization showed that UVC-induced aggregation typically produced a slight increase in the concentration of hydroxyl and carbonyl functionalities, in contrast to the consistent decrease in carboxyl group density. In principle, FTIR could also identify changes in functional group distribution, although in previous studies we have shown that for MWCNTs at least, large changes in oxygen-functional group distribution do not translate into measurable changes in FTIR spectra.<sup>32, 33</sup>

The results shown in Figure 4 and Table S2 provide compelling evidence that the UVC-induced aggregation of O-MWCNTs is caused by a PDC process, since it is the negatively charged carboxylic acid groups are principally responsible for the colloidal stability of O-MWCNTs. Previous studies have revealed that O-MWCNT stability is strongly dependent on the

concentration of surface bound carboxylic acid groups.<sup>30</sup> As UVC irradiation proceeds, the concentration of carboxylic acid groups decreases systematically until a sufficient number of these groups, and thus the negative charge on the O-MWCNTs, have been removed. This process results in a point where the O-MWCNTs are no longer colloiddally stable and begin to aggregate (see Figure 1). The extent of decarboxylation necessary to induce aggregation will depend on the solution conditions. This provides a rationale for the data shown in Figure 3, where the resistance of O-MWCNTs towards UVC induced-aggregation increases under solution conditions that favor the stability of negatively charged colloids (i.e. low ionic strength and high pH). The increasing loss of carboxylic acid groups that occurs as the irradiation time increases also rationalizes the changes in particle concentration and size observed in Figure 2.

To better understand the mechanism of PDC, a kinetic study of UVC-induced aggregation was performed as a function of light intensity by varying the number of lamps in the Rayonet photoreactor. Figure 5 shows that the irradiation time needed to affect UVC-induced aggregation increases systematically as the number of lamps decreases, approximately doubling as the number of lamps is decreased by a factor of two (16 to 8, 8 to 4, 4 to 2), except for a smaller relative change in going from 4 to 2 lamps. The variations in particle concentration by UV-Vis, or particle size by DLS as a function of irradiation time cannot be used directly for a kinetic analysis as they provide an indirect measure of the extent of reaction. However, kinetics dictates that the time taken to reach a common point in the transformation (photodecarboxylation) process amongst different experiments will be inversely proportional to  $k_{eff}$ <sup>38</sup> as long as the initial particle concentration and solution conditions are kept constant. This criterion is satisfied in Figure 5 by ensuring that the initial absorbance, pH and ionic strength are constant. Consequently, in these experiments the time taken to reach a common point in the reaction profile will be directly proportional to the effective rate constant ( $k_{eff}$ ). In Figure 5 we choose the irradiation time taken for the O-MWCNT suspension to decrease to half of its initial absorbance value (A.U. = 0.17; Figure 5C) and for the particle size to increase in effective hydrodynamic diameter to 630nm (Figure 5D) as examples of common points in the reaction profile that can be measured with reasonable degrees of accuracy. Most importantly, if  $n$  is the number of photons involved in the rate determining step that leads to PDC then  $k_{eff}$  will be directly proportional to  $I^n$ , where  $I$  is the intensity of light (which is directly proportional to the number of UV lamps). Under these conditions we can write;

$$t_{0.17} \text{ or } t_{630nm} \propto \frac{1}{k_{eff}} \propto \frac{1}{I^n} \quad \text{Eq. 1}$$

$$\therefore \log t_{0.17} \text{ or } \log t_{630nm} \propto -n \log I \propto -n \log(\# \text{ UV bulbs}) \quad \text{Eq. 2}$$

$t_{0.17}$  and  $t_{630nm}$  represent the irradiation times required for the particle concentration to decrease to 0.17 absorbance units or the particle size to increase to 630nm, respectively. Thus, a plot of  $\log(t_{0.17})$  or  $\log(t_{630nm})$  as a function of  $\log(\# \text{ UV lamps})$  should be linear with a gradient of  $-n$ . Analysis of Figures 5C and 5D shows these two log-log relationships are close to linear ( $R^2 = 0.95$  for 5C and  $0.96$  for 5D) with slopes of  $-0.89$  and  $-0.92$  respectively. Since photon induced processes require an integral number of photons our results indicate that UVC photoinduced decarboxylation is initiated by a single photon process.

Additional mechanistic insights into the PDC process were obtained by examining the effect of dissolved oxygen on the stability of O-MWCNT suspensions towards UVC-induced

aggregation. Figure 6 shows the absorbance and particle size measurements taken for experiments performed at the same pH and ionic strength, but under oxic (open squares) and anoxic (filled circles) conditions. A comparison of the effect of UVC irradiation on O-MWCNTs in nitrogen purged and oxygen saturated solutions revealed essentially identical behaviors at the pH and ionic strength condition examined. Both systems exhibited a decrease in colloidal O-MWCNT concentration (Fig. 6A) with a corresponding increase in particle size (Fig. 6B) after approximately 5hrs of UVC irradiation. Separate measurements (Figure S7) revealed that the concentration of DO in the oxygen saturated solutions was ~3.5 times greater than the level in the nitrogen purged solutions. This invariance to the level of DO was verified in repeated experiments conducted under different solution conditions. These results indicate that the rate of photo-induced aggregation is independent of the dissolved oxygen content, suggesting that the PDC process does not involve reactive oxygen species (such as  $\bullet\text{OH}$ ), which should change in concentration as the dissolved oxygen concentration changes.<sup>39-41</sup>

Collectively, results from the light intensity and dissolved oxygen experiments suggest a PDC mechanism that involves a direct single photon excitation of the carboxylic acid group that triggers the expulsion of  $\text{CO}_2$ . This mechanism is the same as the one proposed using laser flash photolysis,<sup>42</sup> UV irradiation experiments performed in a Rayonet photochemical reactor,<sup>43</sup> and DFT calculations<sup>44</sup> where aliphatic or aromatic acids and esters such as ketoprofen, acetyl phenyl acetic acid, and their derivatives were exposed to a range of UV irradiation wavelengths (254 – 300 nm). These studies have shown that photoexcitation promotes the molecule to an excited singlet state, which expels  $\text{CO}_2$  as it undergoes a rapid intersystem crossing to a triplet state. Before relaxing back to a ground state configuration, the available radical or ionic species extract hydrogen from a neighboring carbon atom or the surrounding medium.

Scheme 1 shows an example from the organic photochemistry literature of PDC from 5*H*-dibenzo[*a,d*]cyclohepten-5-carboxylic acid,<sup>45</sup> a reasonable representation of the local chemical environment for carboxylic acids attached to CNT sidewalls. In this study, the authors concluded that benzannelated acetic acids undergo PDC rapidly from a singlet excited state, proceeding through a carbanion intermediate. Experiments performed in  $\text{D}_2\text{O}$  proved that the hydrogen captured upon returning to the ground state was from the surrounding medium because the carbanion incorporated deuterium at the position vacated by  $\text{CO}_2$ . A review of the organic photochemistry literature on other small acid molecules shows that PDC can occur when a carboxylic acid is protonated or deprotonated, in aqueous or organic solvents. Depending on the conditions (pH, oxic vs. anoxic) and solvent type, PDC proceeds through either ionic (heterolytic cleavage)<sup>42, 43</sup> or radical (mesolytic cleavage)<sup>42, 44</sup> intermediates, which have been monitored by analytical techniques such as transient absorption, fluorescence, mass spectrometry, and NMR. A more detailed explanation of carboxylic acid and ester PDC can be found in the review article by Budac and Wan.<sup>46</sup> This substantive body of organic photochemistry literature leads us to propose the process described in Scheme 2 for PDC and subsequent aggregation of O-MWCNTs.

Our assertion is that reactive oxygen species are not responsible for the photoreduction process exhibited by O-MWCNTs based on the diversity of chemical environments under which PDC can occur. The idea that strongly oxidizing ROS, such as hydroxyl radicals, are responsible for a net reduction process such as PDC is hard to rationalize from an intuitive chemical perspective. Moreover, such a mechanism is inconsistent not only with our experimental observations at different concentrations of dissolved oxygen, but also the extensive body of

already existing organic photochemistry literature which has identified the mechanism, including the fact that PDC can occur in organic solvents where ROS would not exist.<sup>42-44</sup>

In more general terms it should be noted, however, that although the changes in particle size and absorbance values can be ascribed to PDC, the effects of UV irradiation are not restricted to the carboxylic acid groups. For example, photo-induced decarboxylation of ester groups<sup>46</sup> and the photoreduction of ethers<sup>22</sup> (the later demonstrated in the photochemistry of graphene oxide) would be consistent with the significant decrease in the concentration of “other” oxides (not hydroxyl, carbonyl or carboxyl) that chemical derivatization cannot assay (see Figure 4). In this respect, a potential role for reactive oxygen species (such as hydroxyl radicals) that are produced as a result of UV exposure to oxidized CNTs<sup>23, 24</sup> could be the cause of the increase seen in hydroxyl group density. Thus, the chemical transformations to O-MWCNTs induced by UVC irradiation are likely a result of more than one process, though PDC is the dominant process that directly influences particle stability and governs the fate and transport properties of the O-MWCNTs.

#### *Structural Transformations to O-MWCNTs*

To determine if there were any structural transformations imparted to the O-MWCNTs as a consequence of UVC irradiation, TEM and Raman were performed on O-MWCNTs before and after UVC-induced aggregation. TEM images (Figure 7) revealed an absence of any obvious structural changes to the O-MWCNTs after UVC exposure, with the shape, size, and number of sidewalls remaining constant based on visual observations of different O-MWCNTs. Some amorphous carbon can be seen attached to the outer walls of the individual CNTs in both sets of micrographs, with perhaps slightly more on the outer walls of the tubes after UVC irradiation. TEM analysis was performed on a number of O-MWCNTs before and after UVC irradiation under different solution conditions (pH, dissolved gas) with the same qualitative finding. The lack of physical transformations to the surface of O-MWCNTs in our irradiation experiments is similar to the observations of Hwang *et. al.* when they irradiated carboxylated MWCNTs for seven days under UVA light.<sup>25</sup>

Raman spectroscopy was performed on O-MWCNTs that had not been exposed to UVC irradiation (control), as well as suspensions that had been UVC irradiated under oxic and anoxic conditions for sufficient times to induce aggregation. In Raman experiments, O-MWCNTs from two different manufacturers, NanoLab, Inc. and Cheaptubes (Figure 8), were studied. Prior to irradiation, O-MWCNTs from both manufacturers exhibited significant D-band intensities indicative of a large amount of disordered ( $sp^2$ ) carbon atoms, presumably as a result of the aggressive oxidizing conditions needed to introduce surface oxides into the graphenic sidewalls.<sup>47</sup> The NanoLab, Inc. CNTs exhibited identical  $I_D:I_G$  band ratios of 0.94 for the control samples and for O-MWCNTs which had aggregated under the influence of UVC irradiation in a nitrogen purged suspension. The  $I_D:I_G$  band ratio did increase slightly to 1.01 when O-MWCNTs were subjected to UVC irradiation in a solution saturated with dissolved oxygen. In comparison, the Cheaptubes O-MWCNTs  $I_D:I_G$  band ratio increased slightly from 1.17 in the control, to 1.22 after UVC-induced aggregation in either oxic or anoxic conditions. Collectively, these Raman results indicate that UVC induced aggregation proceeds in the absence of any significant structural changes, consistent with the TEM data shown in Figure 7. The very modest increases in  $I_D:I_G$  band ratio observed upon UVC irradiation could potentially be damage resulting from

reactions between ROS generated from irradiation of the suspension and the graphenic portions of CNT sidewalls. It should be noted that the lack of structural changes to the O-MWCNTs is also consistent with an insignificant role for ROS, such as hydroxyl radicals, in the overall photochemical transformation process.<sup>41, 48</sup> In summary, results from TEM and Raman indicate that the significant changes in the O-MWCNT surface chemistry caused by UVC irradiation are not accompanied by any measurable changes to the physical structure of O-MWCNTs.

This absence of any significant structural changes to the O-MWCNTs is also consistent with the comparative lack of mineralization observed (Table 1). In large batch studies greater than 90% of the initial mass was recovered after aggregation, regardless of the solution conditions, time of irradiation, source of O-MWCNTs, or whether the CNTs were cleaned before use. Our results indicate that PDC will occur for all O-MWCNTs regardless of origin, structure or chemical composition. The small amount of mass loss could potentially be ascribed to the CO<sub>2</sub> evolution that accompanies PDC and the concomitant release of a small amount of dissolved organic carbon from destruction of the O-MWCNT sidewalls. The presence of dissolved organic carbon could also be the reason for the slight increase in amorphous carbon observed after irradiation by TEM (see Figure 7).

#### *Phototransformations of Oxidized Carbon Based Nanomaterials*

Our results show similar chemical changes to studies from Hwang *et. al.*<sup>25</sup> and Qu *et. al.*,<sup>26</sup> who irradiated the same O-MWCNTs used in this study with UVA light. Specifically, the three studies saw a photoreduction process that occurred in the absence of significant changes to the material's physical structure. In essence the removal of oxygen functional groups simply causes the particle to become unstable in aqueous solution. The magnitude of the van der Waals attraction between the carbon cores causes aggregation once enough carboxylic acid groups are removed. Consequently, UVC light is unable to effect mineralization of O-MWCNTs because the central carbon core of the O-MWCNTs remains unaffected. A significant difference between our studies and those of Qu *et. al.*,<sup>26</sup> however, comes from the mechanism used to explain the PDC process. Qu *et. al.* postulate that hydroxyl radicals were responsible for decarboxylation in a proposed reaction where a carboxylic acid combines with a hydroxyl radical to produce a molecule of CO<sub>2</sub> and water. Meanwhile, results from our study and from existing organic photochemistry studies indicate that PDC occurs in both oxic and anoxic conditions, as well as in organic solvents where hydroxyl radicals could not exist. Together, these results are inconsistent with a PDC mechanism that involves ROS.<sup>42-46</sup> In more general terms, we believe that we can draw parallels between many environmental transformation processes experienced by nanomaterials and more traditional chemicals that have analogous chemical properties.

In addition to O-MWCNTs, a variety of UV irradiation studies have been performed on other types of oxidized carbon based nanomaterials, such as fullerols and graphene oxide (GO) nanosheets. For O-MWCNTs, the process is dominated by transformations that occur at the surface. If we extrapolate this process to GO nanosheets or fullerols then we would predict that irradiation would have a much greater relative effect since all of the atoms are at the surface of these nanomaterials. Consistent with this assertion, previous studies have reported decreases in the particle size of fullerols by DLS and TEM as a result of UV irradiation, with measurable amounts of CO<sub>2</sub> released that indicate almost 50% mineralization of the fullerol molecule.<sup>49</sup> This suggests that regardless of the carbon based nanomaterial the effect of photolysis is restricted to

species in the uppermost surface layer. An interesting corollary of this assertion is that significant mineralization of O-SWCNTs may be possible under certain photolysis conditions.

An illustrative example of how the details of photolysis depends on the type of oxidized carbon based nanomaterial can be seen if we compare the data obtained for O-MWCNTs to studies on GO nanosheets. In terms of the chemical transformations, GO nanosheet suspensions<sup>17, 19-21</sup> show a similar reduction in surface oxygen concentration to O-MWCNTs. However, the type and amount of oxygen-containing functional groups are different between these two oxidized carbon species, where O-MWCNTs possess a much higher percentage of carboxylic acids and the GO surface is dominated by epoxides in strained geometrical arrangement, result from the different oxidation methods used.<sup>50, 51</sup> Peak fitting of the XPS carbon envelopes by Matsumoto, Guardia, and Koinuma showed almost complete loss of the C-O peak. Thus, photoreduction appears to be a general phenomenon for oxidized carbon based nanomaterials, occurring to a range of different surface oxides depending on the type of nanomaterial. However, the effects of these photoreduction processes produce very different effects on O-MWCNTs and GO nanosheets. Minimal structural damage was observed for O-MWCNTs in the present study as well as those conducted by Hwang *et. al.*<sup>25</sup> and Qu *et. al.*,<sup>26</sup> while AFM micrographs and TEM images of GO nanosheets show distinct holes created by the removal of oxygen.

#### *Environmental Implications*

Results from our study have shown that UVC irradiation can destabilize a colloidal suspension of O-MWCNTs regardless of solution conditions. Many facilities across the country have implemented UVC irradiation to disinfect their water resources. However, these municipal drinking and wastewater treatment plants operate at a multitude of volumes, ranging from 1 – 450 million gallons per day.<sup>52</sup> Even if the UV light intensity in a commercial water treatment plant is an order of magnitude higher than the experiments described in this study (photon flux ~  $1.32 \times 10^{17}$  quanta/sec with all lamps operational), if we consider the volumes of water that must be disinfected each day in one of these plants it seems unlikely that UVC treatment will transform O-MWCNTs to an appreciable extent given the timescales (hours) required for PDC.

## Conclusions

UVC irradiation transformed O-MWCNTs principally through a photodecarboxylation process. This process was found to be mediated by a one photon, direct excitation mechanism consistent with existing literature in the organic photochemistry community, and inconsistent with a process mediated by reactive oxygen species. During the initial stages of irradiation the extent of carboxylic acid group removal from the surface of the O-MWCNTs leads to a slow increase in particle size, but is not sufficient to cause settleable aggregates to form. During this time, the particle concentration remains constant and the suspension remains visibly unchanged to the naked eye. However, once a sufficient number of carboxylic acid groups have been removed, a critical point is reached where the electrostatic repulsion between O-MWCNTs is no longer sufficient to prevent the CNTs from rapidly aggregating. UVC-induced aggregation occurs at all light intensities studied and under both oxic and anoxic conditions where the resistance of O-MWCNTs towards photo-induced aggregation is enhanced in solution conditions that favor the stabilization of negatively charged colloids (high pH and low ionic strength). XPS, Raman, and TEM show significant changes in surface chemistry and aggregation state induced by UVC exposure, but an absence of any discernible structural transformations or significant mineralization.

## Acknowledgments

We acknowledge financial support by the Environmental Protection Agency (R834858). The authors would also like to thank Ken Livi of the Earth and Planetary Sciences Department at JHU for the TEM imaging, and the Materials Science Department at JHU for use of the surface analysis laboratory. JLB would also like to thank Miranda Gallagher for the photos of O-MWCNT suspensions, as well as her and Ronald Lankone's help cleaning and processing CNT samples. SB would like to thank Dr. Yong P. Chen at Purdue's Physics department for the use of their Raman spectroscopy system.

## Appendix

*Supporting Information* includes information regarding UV-Vis spectra, the use of a phosphate buffer, calibrating the Rayonet reaction chamber with actinometry, and dissolved oxygen measurements.

## References

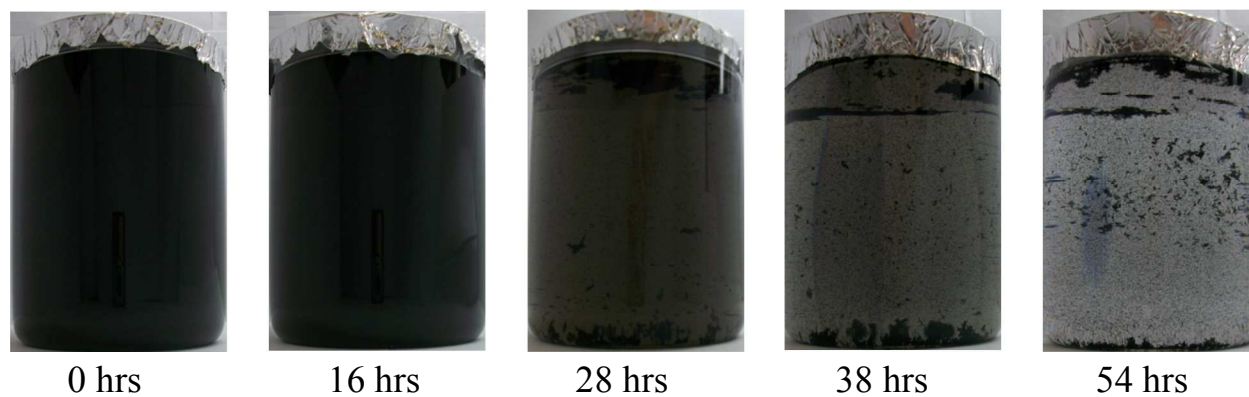
1. D. Hristozov and I. Malsch, Hazards and Risks of Engineered Nanoparticles for the Environment and Human Health, *Sustainability*, 2009, **1**, 1161-1194.
2. G. V. Lowry and E. A. Casman, in *Nanomaterials: Risks and Benefits*, eds. I. Linkov and J. Steevens, Springer Netherlands, Editon edn., 2009, pp. 125-137.
3. K. M. Metz, A. N. Mangham, M. J. Bierman, S. Jin, R. J. Hamers and J. A. Pedersen, Engineered Nanomaterial Transformation under Oxidative Environmental Conditions: Development of an in vitro Biomimetic Assay, *Environmental Science & Technology*, 2009, **43**, 1598-1604.
4. M. R. Wiesner, G. V. Lowry, K. L. Jones, J. M. F. Hochella, R. T. Di Giulio, E. Casman and E. S. Bernhardt, Decreasing Uncertainties in Assessing Environmental Exposure, Risk, and Ecological Implications of Nanomaterials, *Environmental Science & Technology*, 2009, **43**, 6458-6462.
5. B. Nowack, J. F. Ranville, S. Diamond, J. A. Gallego-Urrea, C. Metcalfe, J. Rose, N. Horne, A. A. Koelmans and S. J. Klaine, Potential scenarios for nanomaterial release and subsequent alteration in the environment, *Environmental Toxicology and Chemistry*, 2011, **31**, 50-59.
6. E. J. Petersen, L. Zhang, N. T. Mattison, D. M. O'Carroll, A. J. Whelton, N. Uddin, T. Nguyen, Q. Huang, T. B. Henry, R. D. Holbrook and K. L. Chen, Potential Release Pathways, Environmental Fate, And Ecological Risks of Carbon Nanotubes, *Environmental Science & Technology*, 2011, **45**, 9837-9856.
7. G. V. Lowry, K. B. Gregory, S. C. Apte and J. R. Lead, Transformations of Nanomaterials in the Environment, *Environmental Science & Technology*, 2012, **46**, 6893-6899.
8. G. E. Batley, J. K. Kirby and M. J. McLaughlin, Fate and Risks of Nanomaterials in Aquatic and Terrestrial Environments, *Accounts of Chemical Research*, 2013, **46**, 854-862.
9. M. A. Maurer-Jones, I. L. Gunsolus, C. J. Murphy and C. L. Haynes, Toxicity of Engineered Nanoparticles in the Environment, *Analytical Chemistry*, 2013, **85**, 3036-3049.
10. I. A. Mudunkotuwa, J. M. Pettibone and V. H. Grassian, Environmental Implications of Nanoparticle Aging in the Processing and Fate of Copper-Based Nanomaterials, *Environmental Science & Technology*, 2012, **46**, 7001-7010.
11. J. Lee, M. Cho, J. D. Fortner, J. B. Hughes and J.-H. Kim, Transformation of Aggregated C60 in the Aqueous Phase by UV Irradiation, *Environmental Science & Technology*, 2009, **43**, 4878-4883.
12. Y. S. Hwang and Q. Li, Characterizing Photochemical Transformation of Aqueous nC60 under Environmentally Relevant Conditions, *Environmental Science & Technology*, 2010, **44**, 3008-3013.
13. W.-C. Hou and C. T. Jafvert, Photochemical Transformation of Aqueous C60 Clusters in Sunlight, *Environmental Science & Technology*, 2009, **43**, 362-367.

14. T. Savage, S. Bhattacharya, B. Sadanadan, J. Gaillard, T. M. Tritt, Y.-P. Sun, Y. Wu, S. Nayak, R. Car, N. Marzari, P. M. Ajayan and A. M. Rao, Photoinduced oxidation of carbon nanotubes, *Journal of Physics: Condensed Matter*, 2003, **15**, 5915.
15. N. T. Alvarez, C. Kittrell, H. K. Schmidt, R. H. Hauge, P. S. Engel and J. M. Tour, Selective Photochemical Functionalization of Surfactant-Dispersed Single Wall Carbon Nanotubes in Water, *Journal of the American Chemical Society*, 2008, **130**, 14227-14233.
16. S. H. Lee, Y. C. Jung, Y. A. Kim, H. Muramatsu, K. Teshima, S. Oishi and M. Endo, Optical spectroscopic studies of photochemically oxidized single-walled carbon nanotubes, *Nanotechnology*, 2009, **20**, 105708.
17. Y. Matsumoto, M. Koinuma, S. Ida, S. Hayami, T. Taniguchi, K. Hatakeyama, H. Tateishi, Y. Watanabe and S. Amano, Photoreaction of Graphene Oxide Nanosheets in Water, *The Journal of Physical Chemistry C*, 2011, **115**, 19280-19286.
18. V. A. Smirnov, A. A. Arbuzov, Y. M. Shul'ga, S. A. Baskakov, V. M. Martynenko, V. E. Muradyan and E. I. Kresova, Photoreduction of graphite oxide, *High Energy Chemistry*, 2011, **45**, 57-61.
19. T.-F. Yeh, F.-F. Chan, C.-T. Hsieh and H. Teng, Graphite Oxide with Different Oxygenated Levels for Hydrogen and Oxygen Production from Water under Illumination: The Band Positions of Graphite Oxide, *The Journal of Physical Chemistry C*, 2011, **115**, 22587-22597.
20. L. Guardia, S. Villar-Rodil, J. I. Paredes, R. Rozada, A. Martínez-Alonso and J. M. D. Tascón, UV light exposure of aqueous graphene oxide suspensions to promote their direct reduction, formation of graphene-metal nanoparticle hybrids and dye degradation, *Carbon*, 2012, **50**, 1014-1024.
21. M. Koinuma, C. Ogata, Y. Kamei, K. Hatakeyama, H. Tateishi, Y. Watanabe, T. Taniguchi, K. Gezuhara, S. Hayami, A. Funatsu, M. Sakata, Y. Kuwahara, S. Kurihara and Y. Matsumoto, Photochemical Engineering of Graphene Oxide Nanosheets, *The Journal of Physical Chemistry C*, 2012, **116**, 19822-19827.
22. A. L. Stroyuk, N. S. Andryushina, N. D. Shcherban', V. G. Il'in, V. S. Efanov, I. B. Yanchuk, S. Y. Kuchmii and V. D. Pokhodenko, Photochemical reduction of graphene oxide in colloidal solution, *Theoretical and Experimental Chemistry*, 2012, **48**, 2-13.
23. C.-Y. Chen and C. T. Jafvert, Photoreactivity of Carboxylated Single-Walled Carbon Nanotubes in Sunlight: Reactive Oxygen Species Production in Water, *Environmental Science & Technology*, 2010, **44**, 6674-6679.
24. C.-Y. Chen and C. T. Jafvert, The role of surface functionalization in the solar light-induced production of reactive oxygen species by single-walled carbon nanotubes in water, *Carbon*, 2011, **49**, 5099-5106.

25. Y. S. Hwang, X. Qu and Q. Li, The role of photochemical transformations in the aggregation and deposition of carboxylated multiwall carbon nanotubes suspended in water, *Carbon*, 2013, **55**, 81-89.
26. X. Qu, P. J. J. Alvarez and Q. Li, Photochemical Transformation of Carboxylated Multiwalled Carbon Nanotubes: Role of Reactive Oxygen Species, *Environmental Science & Technology*, 2013, **47**, 14080-14088.
27. B. Smith, J. Yang, J. L. Bitter, W. P. Ball and D. H. Fairbrother, Influence of Surface Oxygen on the Interactions of Carbon Nanotubes with Natural Organic Matter, *Environmental Science & Technology*, 2012, **46**, 12839-12847.
28. S. n. Fogden, R. Verdejo, B. Cottam and M. Shaffer, Purification of single walled carbon nanotubes: The problem with oxidation debris, *Chemical Physics Letters*, 2008, **460**, 162-167.
29. C. G. Salzman, S. A. Llewellyn, G. Tobias, M. A. H. Ward, Y. Huh and M. L. H. Green, The Role of Carboxylated Carbonaceous Fragments in the Functionalization and Spectroscopy of a Single-Walled Carbon-Nanotube Material, *Advanced Materials*, 2007, **19**, 883-887.
30. B. Smith, K. Wepasnick, K. E. Schrote, H.-H. Cho, W. P. Ball and D. H. Fairbrother, Influence of Surface Oxides on the Colloidal Stability of Multi-Walled Carbon Nanotubes: A Structure-Property Relationship, *Langmuir*, 2009, **25**, 9767-9776.
31. C. G. Hatchard and C. A. Parker, A New Sensitive Chemical Actinometer. II. Potassium Ferrioxalate as a Standard Chemical Actinometer, *Proc. R. Soc. Lond. A.*, 1956, **235**, 518-536.
32. L. A. Langley, D. E. Villanueva and D. H. Fairbrother, Quantification of Surface Oxides on Carbonaceous Materials, *Chemistry of Materials*, 2005, **18**, 169-178.
33. K. A. Wepasnick, B. A. Smith, K. E. Schrote, H. K. Wilson, S. R. Diegelmann and D. H. Fairbrother, Surface and structural characterization of multi-walled carbon nanotubes following different oxidative treatments, *Carbon*, 2011, **49**, 24-36.
34. X. S. Wang, P. Liu, H. T. Zheng, H. Hu, W. J. Zheng and S. I. Suye, Preparation of Nicotinamide Adenine Dinucleotide Functionalized Multi-Walled Carbon Nanotube and its Application to Dehydrogenase Biosensor, *Advanced Matieral Research*, 2011, **298**, 121-127.
35. E. V. Anslyn and D. A. Dougherty, *Modern Physical Organic Chemistry*, University Science Books, Sausalito, CA, 2006
36. V. D. Noto and M. Mecozzi, Determination of Seawater Salinity by Ultraviolet Spectroscopic Measurements, *Applied Spectroscopy*, 1997, **51**, 1294-1302.
37. H.-H. Cho, K. Wepasnick, B. A. Smith, F. K. Bangash, D. H. Fairbrother and W. P. Ball, Sorption of Aqueous Zn[II] and Cd[II] by Multiwall Carbon Nanotubes: The Relative Roles of Oxygen-Containing Functional Groups and Graphenic Carbon, *Langmuir*, 2010, **26**, 967-981.
38. P. Atkins and J. de Paula, *Physical Chemistry*, 7th edn., W. H. Freeman and Company, New York, 2002

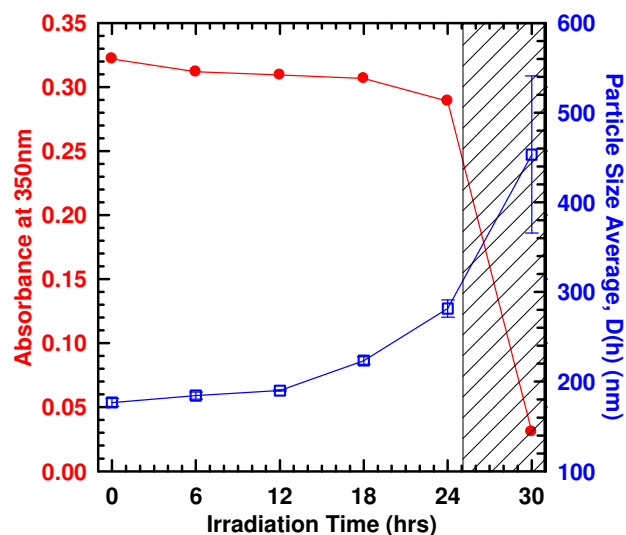
39. M. Cho, H. Chung, W. Choi and J. Yoon, Linear correlation between inactivation of *E. coli* and OH radical concentration in TiO<sub>2</sub> photocatalytic disinfection, *Water Research*, 2004, **38**, 1069-1077.
40. C. B. Almquist and P. Biswas, A mechanistic approach to modeling the effect of dissolved oxygen in photo-oxidation reactions on titanium dioxide in aqueous systems, *Chemical Engineering Science*, 2001, **56**, 3421-3430.
41. W. R. Haag and J. Hoigné, Photo-sensitized oxidation in natural water via •OH radicals, *Chemosphere*, 1985, **14**, 1659-1671.
42. L. J. Martínez and J. C. Scaiano, Transient Intermediates in the Laser Flash Photolysis of Ketoprofen in Aqueous Solutions: Unusual Photochemistry for the Benzophenone Chromophore, *Journal of the American Chemical Society*, 1997, **119**, 11066-11070.
43. M. Xu and P. Wan, Efficient photodecarboxylation of aroyl-substituted phenylacetic acids in aqueous solution: a general photochemical reaction, *Chemical Communications*, 2000, 2147-2148.
44. L. Ding and W.-H. Fang, Exploring Photoinduced Decarboxylation Mechanism of *o*-Acetylphenylacetic Acid from the Combined CAS/SCF and DFT Studies, *The Journal of Organic Chemistry*, 2010, **75**, 1630-1636.
45. I. McAuley, E. Krogh and P. Wan, Carbanion intermediates in the photodecarboxylation of benzannulated acetic acids in aqueous solution, *Journal of the American Chemical Society*, 1988, **110**, 600-602.
46. D. Budac and P. Wan, Photodecarboxylation: mechanism and synthetic utility, *Journal of Photochemistry and Photobiology A: Chemistry*, 1992, **67**, 135-166.
47. K. A. Wepasnick, B. A. Smith, J. L. Bitter and D. H. Fairbrother, Chemical and structural characterization of carbon nanotube surfaces, *Analytical and Bioanalytical Chemistry*, 2010, **396**, 1003-1014.
48. X. Wang, X. Huang, C. Zuo and H. Hu, Kinetics of quinoline degradation by O<sub>3</sub>/UV in aqueous phase, *Chemosphere*, 2004, **55**, 733-741.
49. L. Kong, O. N. Tedrow, Y. F. Chan and R. G. Zepp, Light-Initiated Transformations of Fullerenol in Aqueous Media, *Environmental Science & Technology*, 2009, **43**, 9155-9160.
50. W. S. Hummers and R. E. Offeman, Preparation of Graphitic Oxide, *Journal of the American Chemical Society*, 1958, **80**, 1339-1339.
51. D. R. Dreyer, S. Park, C. W. Bielawski and R. S. Ruoff, The chemistry of graphene oxide, *Chemical Society Reviews*, 2010, **39**, 228-240.
52. TrojanUV, *UV Resources*, <http://www.trojanuv.com/uvresources>, Accessed December 5, 2013.



**Figure 1**

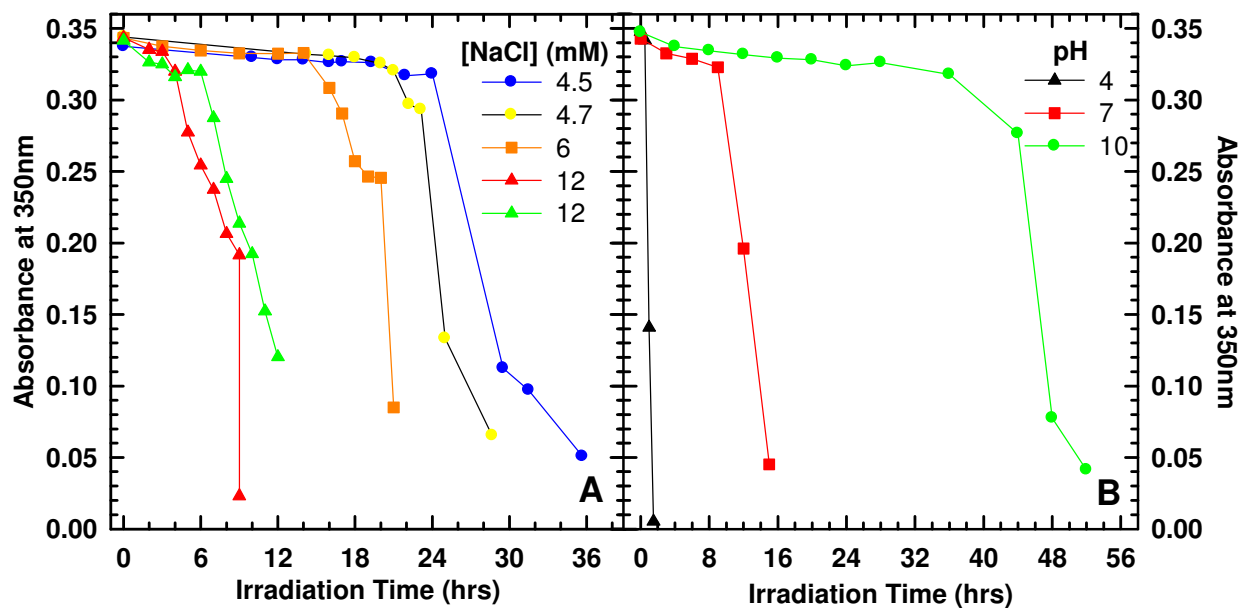
**Figure 1** – Visual effects of UVC irradiation on oxidized multiwalled CNTs from NanoLab, Inc. under anoxic conditions at pH 10 and 3mM Na<sup>+</sup>. No observable change is apparent over the first 18 hours; afterwards aggregation and settling are observed. Starting O-MWCNT concentration is approximately 5mg/L.

Figure 2



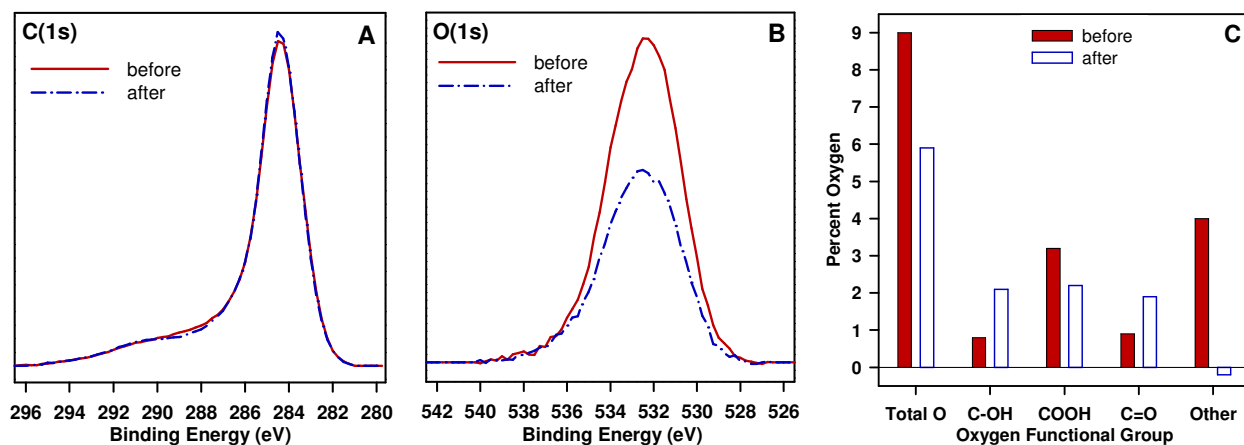
**Figure 2** – Change in absorbance (filled red circles) and particle size (open blue squares) plotted as a function of UVC irradiation time for oxidized multiwalled CNTs under anoxic conditions at pH 7 and 3mM Na<sup>+</sup> under radiation with 8 UVC lamps. The shaded region indicates the time where visible aggregation of CNTs was observed.

Figure 3



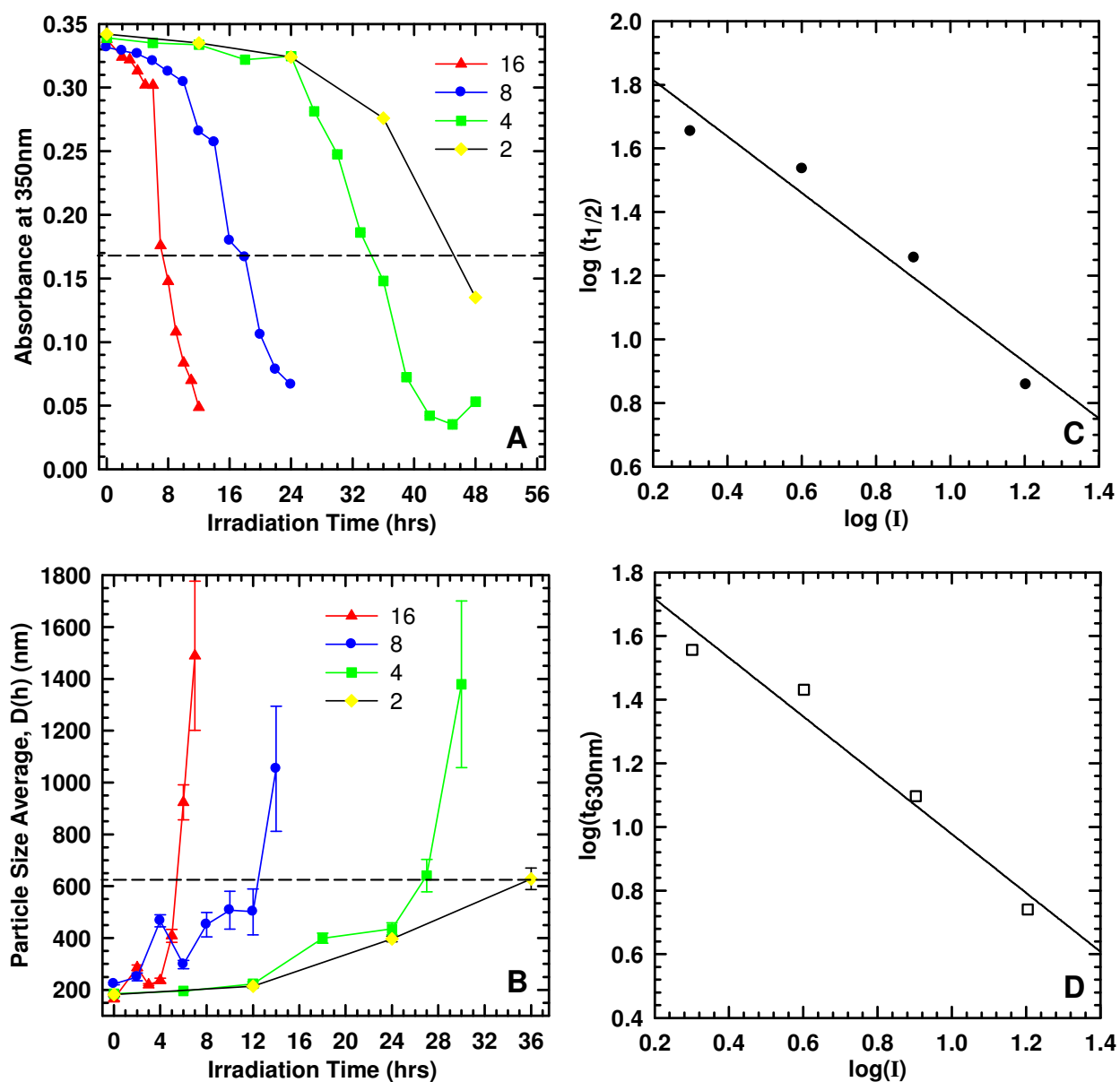
**Figure 3** – Absorbance profiles for oxidized multiwalled CNTs under anoxic conditions as a function of ionic strength at constant pH 7 (A) and pH at constant ionic strength 3mM Na<sup>+</sup> (B) plotted as a function of UVC irradiation time.

Figure 4



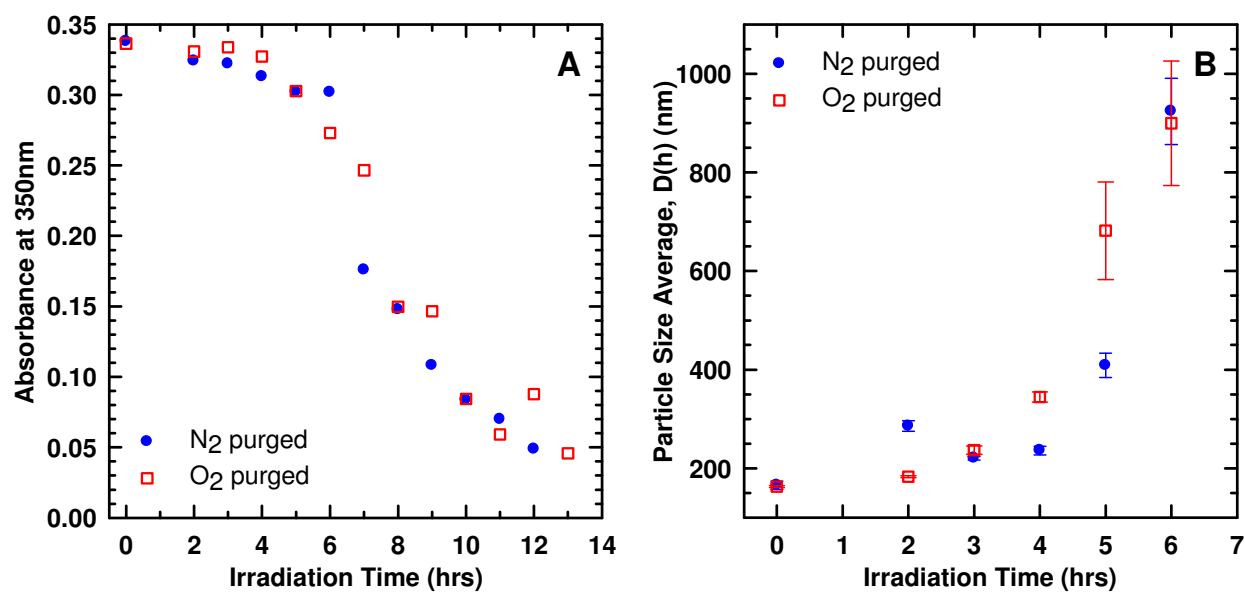
**Figure 4** – XPS results for oxidized multiwalled CNTs in absence of any irradiation (solid red line) and after UVC-induced aggregation and settling had occurred (dashed blue line). The solution conditions in these experiments were 3mM NaCl and pH 10. Figures 4A and 4B show the C(1s) and O(1s) envelopes before and after irradiation. The distribution of oxygen-containing functional groups (C) determined by chemical derivatization illustrates how UVC irradiation changes the concentration of different oxygen-containing functional groups.

Figure 5



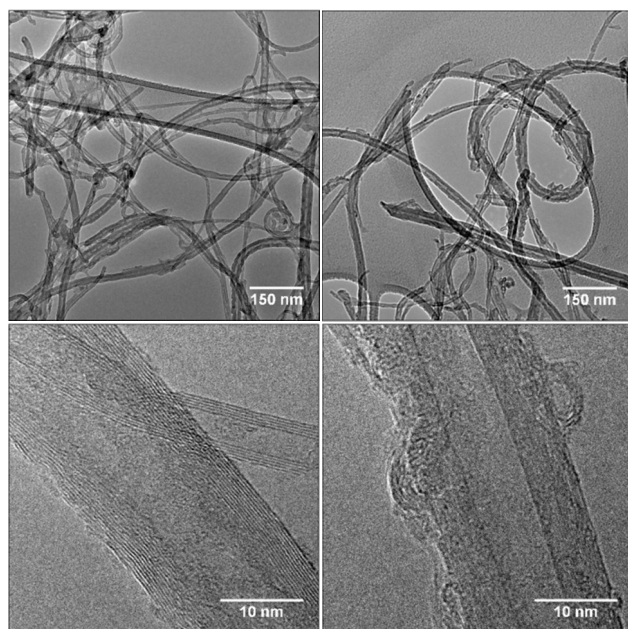
**Figure 5** – Absorbance (A) and particle size (B) profiles for oxidized multiwalled CNTs at pH 7 and 12mM NaCl exposed to different light intensities, plotted as a function of irradiation time. The dashed lines indicate  $t_{1/2}$  (A) where the absorbance reaches half of its initial value, and  $t_{630nm}$  (B) where the particle size reached  $\sim 630nm$ . Kinetic data is plotted as a log-log function of  $t_{1/2}$  (C), or  $t_{630nm}$  (D), versus light intensity ( $I$ ).

Figure 6



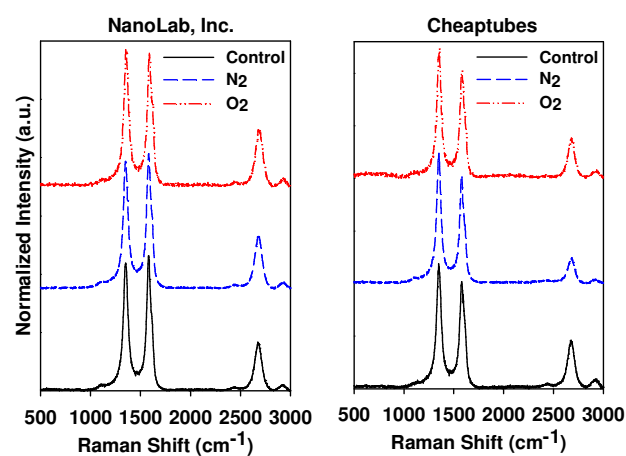
**Figure 6** – Absorbance (A) and particle size (B) profiles for oxidized multiwalled CNTs at pH 7 and 12mM NaCl plotted as a function of UVC irradiation time, conducted under anoxic (nitrogen purged) or oxic (oxygen purged) conditions.

Figure 7



**Figure 7** – Low (top row) and high (bottom row) resolution TEM micrographs of O-MWCNTs before (left) and after (right) UVC irradiation at pH 7 under anoxic conditions.

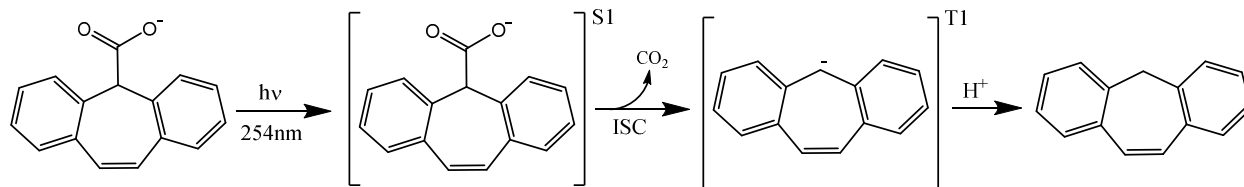
Figure 8



**Figure 8** – Raman spectroscopy showing the effects of UVC irradiation on O-MWCNTs purchased from NanoLab, Inc. and Cheaptubes. Results are shown for O-MWCNTs before irradiation and after UVC-induced aggregation under oxic and anoxic conditions at pH 10.

## Scheme 1

**Scheme 1** – Mechanism for the photodecarboxylation of 5H-dibenzo[a,d]cyclohepten-5-carboxylic acid in water proceeding through a carbanion intermediate upon irradiation with 254nm light based on work by McAuley *et. al.*<sup>42</sup>



## Scheme 2

**Scheme 2** – Proposed pathway for photodecarboxylation and subsequent aggregation of O-MWCNTs through the removal of carboxylic acid functional groups.

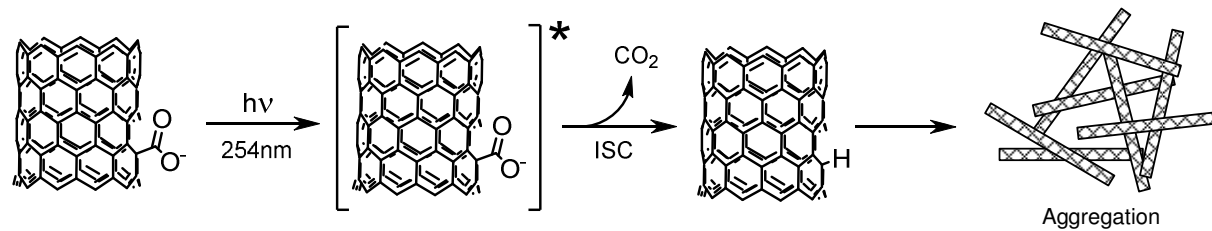


**Table 1**

**Table 1** – Mass loss experienced by O-MWCNTs from NanoLab, Inc. and Cheaptubes as a result of UVC induced aggregation under different solution conditions.

<b>CNT Manufacturer</b>	<b>pH</b>	<b>Purged With</b>	<b>Percent Remaining</b>
<b>NanoLab, Inc.</b>	10	Nitrogen	91%
<b>NanoLab, Inc.</b>	10	Nitrogen	92%
<b>NanoLab, Inc.</b>	10	Oxygen	94%
<b>NanoLab, Inc.</b>	7	Nitrogen	97%
<b>Cheaptubes</b>	10	Oxygen	93%

The effects of high energy UVC light used in drinking and waste water treatment plants on engineered nanomaterials has not been well established. Experimental evidence reveals that UVC irradiation transforms O-MWCNTs principally through a single photon, direct photodecarboxylation process via a mechanism analogous to the removal of CO<sub>2</sub> from organic molecules. UVC induced transformations to O-MWCNTs are driven by changes in the oxygen-containing functional groups at the surface of the O-MWCNTs, in the absence of any significant structural changes or mineralization of the carbon atoms in the core of the O-MWCNT. This information advances our understanding of how engineered nanomaterials can be transformed and supports the general consensus that O-MWCNTs will persist in the environment for extended periods of time.